SM-107/136
Original: RUSSIAN

EXPERIMENTAL INVESTIGATIONS ON LIQUID-METAL MHD GENERATORS

G.A. Baranov, V.F. Vasilyev, V.A. Glukhikh, B.G. Karasev,
I.R. Kirillov and I.V. Lavrentyev
D.V. Efremov Research Institute for Electrophysical Equipment,
Leningrad, USSR

ABSTRACT

The paper reports the results of tests on AC and DC MHD generators. The types of generator involved were plane linear induction generators, and helical and straight-flow DC generators. The trials were carried out under conditions both of independent excitation and self-excitation.

The experimental circuit (apart from the generators themselves) consisted of the requisite tubing, an accelerating device (electromagnetic pump), a heat exchanger, and measuring equipment. The working fluid was an Na-K alloy (78% K) at a temperature of 100-150°C. The maximum parameters were: flow rate 50 m^3/h, pressure 10 kg/cm^2, velocity in the generator ducts 40 m/s, and applied magnetic field in the DC generators 1.43 T. The ducts of all generators were of stainless steel.

The maximum electric power produced by the monopole plane induction generator working under self-excitation conditions was 1160 W, the gross efficiency 16.2%, the efficiency neglecting hydraulic losses in the duct 25.9% and $\cos\varphi = 0.2$. The corresponding figures for a single-wave generator were: power [illegible] W, gross efficiency 4% and efficiency neglecting hydraulic losses 17%. The maximum DC generator parameters when operating with independent excitation were: power 2 kW, current 6 kA and gross efficiency (neglecting excitation losses) 40%; the corresponding figures for the self-excitation regime were [illegible] kA and 30%.

During the tests readings were taken of the no-load and the working characteristics, together with measurements of the hydraulic losses in the ducts and the Joule losses in the working fluid, on the duct walls and in the excitation windings. In addition, during the single-wave generator tests, investigations were made of various methods of compensating the longitudinal boundary effect in the primary circuit, which indicated the possibility of

increasing the efficiency. The tests on the DC generators included measurements of the magnetic field in the gap along the duct. These measurements showed that the distortion of the magnetic field along the duct depends on the magnitude of the applied magnetic field, the velocity of the working fluid and the size of the load.

With a view to optimizing, from the hydraulic point of view, the dimensions and geometry of MHD generator ducts, trials involving the running of water and liquid metal through the parts subject to fluid flow were carried out. In the course of these investigations the flow structure was investigated, the hydraulic losses were assigned to sections longitudinally, the optimum shape of the transition sections were found, and the coefficients of hydraulic resistance were determined.

The experimentally determined electromagnetic values were compared with the corresponding theoretical quantities.

International Atomic Energy Agency

SYMPOSIUM ON THE PRODUCTION OF ELECTRICAL ENERGY BY MEANS OF MHD-GENERATORS
Warsaw, 24-30 July 1968

SM107/136

EXPERIMENTAL INVESTIGATIONS ON LIQUID-METAL MHD GENERATORS

by

G.A. Baranov, V.F. Vasilyev, V.A. Glukhikh, V.G. Karasev,
I.R. Kirillov, and I.V. Lavrentyev

*D.V. Efremov Research Institute for Electrophysical Equipment,
Leningrad, U.S.S.R.*

MHD generators due to the large velocities of the liquid-metal working medium have hydraulic losses in the ducts that comprise a considerable part in the total balance of power. In connection with this, the tendancy has been noted to decrease the length of the operating ducts of the generators. Here, however, end effects more sharply begin to appear associated with the openness of the magnetic system of linear generators, which leads to a sharp deterioration in their operating performance [characteristics]. A number of known methods of improving the performance of short generators are based on the equilization of the magnetic field in the gap of the machine along the duct and in the correct field shaping in the input and output zones of the working medium into the field. These are just the questions that were experimentally investigated on plane AC and DC linear generators. Parallel with them, work was performed in the selection of optimal duct geometry from the point of view of reducing their hydraulic resistance, and generators of the helical type were investigated where the end effects appear considerably weaker.

Experiments were performed in circuits along which fused NaK, Na, or K were pumped by means of electromagnetic pumps; the temperature of the melt was kept constant by means of electric heaters and water heat-exchangers. The velocity of the metal in the working sectors of the ducts reached 20 m/sec, and the pressure developed—25 kg/cm^2. The ducts of all generators were made of stainless steel.

1. Plane linear induction generators.

As is known, due to the openness of the magnetic systems of generators of this type, pulsating and reverse [traveling] [electro-] magnetic fields exist in the working gap in addition to the direct [traveling field]. In connection with this, additional losses of power (primary longitudinal edge effect) arise in the liquid metal. Additional losses of power also appear even in the presence of only the direct fields due to the metal input into the magnetic field and the output from it (secondary edge effect).

Experimental investigations were conducted on a six-pole ($2p = 6$) and

a single-wave ($2p$ = 2) generator. The basic structural data of the six-pole generator are: winding is three-phase two-layer loop (the half-filled slots along the ends of the inductor [magneto] form a seventh pole); the pole separation τ = 180 mm; the width of the duct a = 140 mm and equal to the width of the inductor, height h = 8 mm, wall thickness t_w= 0.8 mm; the gap between the inductors d = 13mm. To reduce the cross-sectional edge effect from the sides, copper bus bars were introduced into the duct located beyond the limits of the inductor. The basic structural data of the two-pole generator are: winding three-phase single-layer, τ = 102 mm; dimensions of the duct a = 69 mm, h = 5.5 mm, t_w = 0.5 mm, d = 10.7 mm; short-circuit bus bars of copper are welded to the side walls of the duct, cross section of the bus bars is 6 × 30 mm^2, and the length 210 mm. The two external slots of the inductor beyond the limits of the winding have compensating [balancing] coils connected so that they form loops that include the active part of the magnetic conductor [wire].

On the six-pole generator questions of self-excitation were examined in the operation with a battery of capacitors connected to the stator winding. The generator was stably excited on attaining the predetermined metal velocity, the value for this was a function of the frequency of the voltage to be generated and the value of the load. Self-excitation also took place in the absence of a residual charge at the capacitors or temperory feeding from a DC source, moreover, artificial demagnetization had no appreciable effect on the length of the self-excitation process and the value of the metal velocity that corresponds to the beginning of self-excitation. The experiment showed that the voltage and current of the generator in the self-excitation process reached established values even in an unsaturated magnetic system and in the absence of any electromagnetic non-linearity, if the mechanical performance of the accelerating device $p(v)$, where p is the pressure and v the velocity, satisfies the predetermined conditions. Specifically, these conditions are always satisfied for the falling $p(v)$ performance of the electromagnetic pump which was used for the acceleration of the metal.

During the tests, different characteristics [performance] of the generator were recorded with a change in the metal velocity, the initial electric power, frequency of the voltage to be generated. The maximum value of the full [total] efficiency at the electric power output P_1 = 1.16 kW is equal to η = 16.2% and electromagnetic efficiency (i.e., without taking into consideration hydraulic losses) is η_{elec} = 29.5%. The experimental values of η_{elec} coincide quite satisfactorily with the theoretical calculations (discrepancies do not exceed 11%). The results of these investigations are presented in more detail in the paper [ref. #1].

In a single-wave generator where the edge effects are more sharply expressed, different methods of compensation of the primary edge effect were investigated. (Compensation of the secondary edge effect was investigated in the paper [ref. #2].) The generator was tested both without compensation and with compensation by two methods: a) compensating coil shorted, b) compensating coil connected in series in a phase that is symmetrical with respect to the middle of the inductor, as was suggested in the

paper [ref. #3]. Here the magnetic field distribution in the gap along the inductor was measured by means of pickup loops (17 × 69 mm) located under the notches [projections] of the inductor. As tests have shown in the no-load mode (without duct) at a phase voltage of 110 volts without compensation of the edge effect, the value of the reverse and pulsating magnetic fields was approximately 30% of the basic traveling field, and with compensation by the indicated methods approximately 20% In the operating mode, with self-excitation by a battery of capacitors connected to the winding terminal, the asymmetry of currents in phases smoothed out somewhat in comparison to the no-load mode. Thus, without compensation at a phase voltage of 110 volts, the value of the pulsating and reverse fields was approximately 20% of the initial, and with compensation by the indicated methods approximately 12%. The distribution curves of the magnetic field in the gap along the length of the inductor are shown in figure 1 for the operating mode of the generators. Dips in the curves are explained by the presence of pulsating and reverse fields, and the different height of the maxima by reaction of the secondary circuit. The reduction of the dip in the curves with compensation in comparison to the case without compensation attests to the decrease in the pulsating and reverse [traveling] fields. Such a degree of the parasitic [spurious] component of the magnetic field leads to a certain increase in efficiency (figure 2). However, as experiments have shown, the most substantial effect of compensation is attained with a matching in phases of capacitances to be used for self-excitation, thus, so that the equality of currents in the phases is provided (figure 2, curve 3). If, simultaneously with this matching of capacitances, compensation by means of short-circuited coils is also used, then the increase in the efficiency becomes still more appreciable. Here, the distribution curve of induction along the length of the generator (figure 1, curve 4) has a more uniform character, and the parasitic components of induction converge to a minimum. The efficiency curve corresponding to this case has form [shape] (4) of figure 2. Thus, this combinational method of compensation made it possible to substantially raise the efficiency of the generator.

All methods examined were used for compensation of the primary longitudinal edge effect. The reduction of losses caused by the openness of the secondary circuit, e.g., by means of erecting insulation partitions in the end zones will apparently make it possible to raise still more the efficiency of the single-wave generator.

2. Helical induction generators. At the small flow rates of the liquid metal and at the large pressures to be developed, asynchronic generators with a helical duct will obviously have definite advantages. The helical generator tested had the following structural data: duct cross section 4.5 × 31 mm , wall thickness 0.4 mm, mean diameter 93.7 mm, number of helices of the duct $n = 5.5$; $2p = 2$, $\tau = 147$ mm. The generator operated with potassium at a temperature of up to 400°C.

Figure 3 shows the operating characteristics, i.e., the current of the generator I_g, the current of the load I_1, the coefficient of power cos φ, the flow rate of the liquid metal Q, slippage S, total efficiency, electromagnetic efficiency, and power supplied to the generator P_2 as a

function of the initial electrical power P_1. The characteristics are obtained in the self-excitation mode at a phase voltage U = 90 V = const, f = 50 Hz = const, and the temperature of the liquid metal 150°C. The maximum initial electrical power was 650 W at full efficiency of 8% and electromagnetic efficiency of 18%.

The theoretical calculation in the assumption of constancy of velocity through the duct's cross section showed that the experimental losses in the liquid metal found by the loss-division method differs subtantially from the calculated. The compilation of losses of power in the liquid metal, relative to the square of the induction and the square of the frequency, is presented in figure 4 for a test of the parallel operation of the generator with the electrical mains of f = 50 Hz. From the figure it is seen that the theoretical and experimental values have a large coincidence at a slippage close to +1, i.e., at small velocities of the liquid metal in the generator duct. When slippage decreases to $S \approx 0.4$, i.e., the velocity increases, the divergence of the theoretical and experimental data increases, after which it remains approximately constant in the range $-0.8 < S < 0.4$.

At the present time experiments have been begun onamore powerful helical generator with sodium (t = 200°C) as a working medium. This generator has the stator of the above described generator and duct dimensions of 7.75 × 35 mm^2. The first experimental data obtained are: initial electrical power 2.7 kW, full efficiency 23.5% at a phase voltage of 220 volts and at a frequency of 50 Hz.

3. DC generator. The energy indices of DC-MHD generators are essentially a function of the character of the magnetic field distribution along the duct. From this point of view it is desirable to have a homogeneous field in the electrode zone and as smooth as possible a decaying field beyond the electrodes. The last requirement is necessary for the reduction of the Julean losses from the parasitic end currents. These losses can also be reduced by introducing into the end zones of the duct non-conducting partitions whose plane is parallel to the flow and the operating [working] component of the magnetic field. Quantitatively, the influence of these effects on the electrical characteristics of the generator can be traced if the formulas for these characteristics are written in the form:

$$P_1 = UI = \frac{\sigma B_0^2 Q^2}{h} k[cG_1 - k\phi' + \beta_1] \tag{1}$$

$$P_2 = p_{elec}Q = \frac{\sigma B_0^2 Q^2}{h}[c(G_2 - kG_1) - k\beta_1 + \beta_2] \tag{2}$$

$$\eta_{elec} = \frac{P_1}{P_2} \tag{3}$$

where P_1, U, I are respectively the power, voltage, and current of the generator taken from the electrodes; P_2, p_{elec}, Q the electromagnetic power, pressure, and flow rate of the metal developed in the duct; η_{elec} the electromagnetic efficiency, σ the conductivity of the liquid metal; $k = \frac{Uh}{B_0 Q}$ the coefficient of load; $\phi' = \left(c + \frac{2 \ln 2}{\pi}\right)\left(1 + \frac{2t_w\sigma_w}{hQ \leftarrow (?)}\right)$ [illegible] electrodes, and the [illegible] current under load [illegible] in the gap and 3 values of poles [illegible] in the no-load and short-circuit modes.

the dimensionless integral conductivity of the duct; B_0 is the magnetic field in the center of the gap; $c = L/a$, L, a, h the length of the electrodes, width and height of the duct; t_w, σ_w the thickness and conductivity of the duct walls. The coefficients G_1 and G_2 characterize the degree of homogeneity of the magnetic field in the electrode zones; G_1 and G_2 respectively are the mean values of the field and its square along the length of the electrodes with respect to B_0. The coefficients β_1 and β_1 describe the effect of the distribution of the magnetic field beyond the electrodes on the characteristics of the generator ($\beta_1 = \beta_2 = 0$, if the field is absent beyond the electrodes) and is a function of the relative polar excess [surplus] $c_* = (L_1-L)/2a$ (L_1 is the length of the pole piece) and the relative air gap $d_* = d/a$ (d is the value of the magnet gap). Figures 5 and 6 show graphs of β_1 and β_2 calculated according to the formula of the paper [ref. #4] on the assumption that the magnetic field is given in the form

$$\frac{B(x)}{B_0} = \begin{cases} 0.83 + 0.17\ (1 - \exp[5.29\ x/d]) & \text{when } x/d < 0 \\ 0.83\ \exp[1.07\ x/d] & \text{when } x/d > 0. \end{cases}$$

The coordinate x is read along the duct; $x < 0$ in the magnet gap, $x > 0$ beyond the pole piece. Since the multiduct generator (ie., generator with partitions) is electrically a series connection of single-channel generators (they are hydraulically parallel), then its characteristics are determined by formulas (1) - (3). In the operating mode it is possible to obtain the most uniform magnetic field in the gap of the electromagnet by means of compensation of the "reaction of the armature" by means of a reverse conductor along which the current flows in a direction opposite to the current in the liquid metal.

For the purpose of experimental verification of the influence of magnetic field distribution on the characteristics of the generator, investigations of a DC generator of independent excitation were conduted. The generator duct was made of 2 thin-walled tubes of rectangular cross section welded to one another on the smaller side along the length of the electrodes and insulated in the external electrode zone. The total length of each duct element is 530 mm, height 8 mm, width 25 mm (total width of the duct 50 mm, length of the electrodes 50 mm). In order to provide mechanical strength, the duct is covered on the outside by a supporting skin. Measurements of the pressure in each duct element were conducted at a distance of 50 mm from the electrodes (at the input of the metal) and 100 mm at the output. The compensation of the "reaction of the armature" was conducted by means of two copper bus bars located in the gap of the magnet above and below the duct. The thickness of the bus bars is 5 mm, the width 50 mm, i.e., equal to the length of the electrodes. The electromagnet had a detachable pole piece making it possible to obtain relative pole excesses $c_* = 0$, 0.8, and 1.6; the height of the air gap $d = 32.8$ mm ($d_* = 1.31$). The magnetic field distribution in the gap (between wall of the duct and bus bar) along the length of the duct was measured by a Hall pickup whose signal was recorded by a self-recording device. During the experiments the following were measured: the pressure gradient in the duct, the flow rate of the metal, the voltage at the electrodes, and the current under load at various values of induction in the gap and 3 values of polar excess. The generator was tested in the no-load and short-circuit modes.

The electrical resistance of the duct without the liquid metal and with the metal was measured first at various temperatures, and according to the data obtained, the mean value of the magnitude $\phi' = 1.06$ was determined. The values of the no-load voltage calculated according to the formula

$$U_{xx} = \frac{B_0 Q}{h} \frac{cG_1+\beta_1}{\phi'} \qquad (4)$$

(which follows from (1) when $P_1 = 0$) agree well with their experimental values presented in figure 7 at various values of B, Q, and c_*. Figure 8 shows the dependence of the pressure gradient in the duct without the magnetic field (Δp_g) and in the no-load mode (Δp). As is seen from the figure, with an increase of the pole excess c_*, the electromagnetic pressure developed $\Delta p_{elec} = \Delta p - \Delta p_g$ grows with an increase of c_*. At the same time, as follows from formula (2), the electromagnetic power developed in the no-load mode in practice is not a function of c_* and is equal to $P_{2xx} \approx 0.18\ \sigma B^2 Q^2/h$. Actually, P_{2xx} is accumulated from two parts.

$P_{1w} = U_{xx}^2\ 2t_w\sigma_w\left(c + \frac{2\ \ln\ 2}{\pi}\right)$ is the power liberated in the conducting walls of the duct, and P'_{2xx} is the Joulean loss in the liquid metal. With an increase in polar excess, P_{1w} grows due to the increase of U_{xx}, and P'_{2xx} falls with the growth of c_* (in the electrode zone $\sim (1 - k_{xx})^2$, and in the end zone due to the removal of the region of nonhomogeneity of the magnetic field from the electrode), so that in our case the value $P_{2xx} = P_{1w} + P'_{2xx}$ remains approximately constant. The divergence of the experimental data noted above from the calculated can be explained by the fact that the formulas used in the calculations of (1)-(3) are based on the solution of a two-dimensional problem; they give satisfactory agreement with the experiment for values that are linear in current (P_1, I, U_{xx}), at the same time for values that are quadratic in current (P_2, P_{xx}) they lead to decreased values. Specifically, in the no-load mode with a growth of c_*, the length of the zone of the homogeneous magnetic field increases and the Joulean losses connected with the closing of the currents in the boundary [edge] layer and on to the conducting walls of the duct increase proportionally to the length of the loss of the magnetic field beyond the electrodes which coincides with the experimental results obtained.

Figures 9, 10, and 11 show the distribution curves of the magnetic field along the duct at various inductions and at three values of pole excess ($c_* = 0$, 0.8, and 1.6), taken when $v = 0$ and $v = 17$ m/sec in the no-load mode. From the figures the insignificant removal of the field is evident in the direction of the flow. In the short-circuited mode, the misalignment of the field along the duct was observed but it was very insignificant which is explained by the quite good compensation of the "reaction of the armature" in spite of the relatively small value of the load current ($I_{max} = 3280$ amp). The maximum power recorded in the short-circuit mode is 103 kW, when $\eta_{elec} = 42.3\%$, current 3280 amp and $c_* = 1.6$; maximum electromagnetic efficiency 48.5% at a plotted power of 0.88 kW, current 3085 amp, and $c_* = 0$.

4. Hydraulic investigations. Experiments with flow circuits of plane linear generators and also calculations in the determination of hydraulic resistances show that the coefficients of resistance change in quite a wide range and are strongly different from the calculated resistances. This occurs due to the fact that the flow circuits of the MHD engines have quite unique geometric shapes (figure 12) and it has not appeared possible to satisfactorily match analogies in determining their hydraulic resistance.

The flows of the flow circuits were made on special [test] stands with a liquid metal and their models with industrial water for the purpose of determining the coefficient of hydraulic resistance, the study of the flow structure, and the distribution of the losses along the length.

The treatment of the investigated flow circuits was first conducted on an aerodynamic stand, the prismatic [knife-edge] section having remained unchanged, and with only the configuration and dimensions of the reducers [adapters, transfer joints] being changed. The character of the flow was studied by means of visual observation of the flow; glowing pieces of wood were introduced for this purpose along with photography.

For all models a dependence was constructed of the total coefficient of hydraulic resistance on the Reynolds number $\zeta = f(\mathrm{Re})$ at 30 to 40 points. The Reynolds number was varied within thelimits of $(2\text{-}10)\cdot 10^4$.

According to the air flow circuits, models were prepared for more detailed study on the hydraulic stand. Geometric dimensions of the models were selected from the conditions of obtaining Reynolds numbers greater than 10^5. The Reynolds numbers were calculated in all cases according to the hydraulic diameter and mean velocity in the tubes feeding the flow.

Piezoelectric pressures were recorded on the prismatic section of the model in six columns along [in] 8 directions, the velocity fields were recorded in two cross sections—at the input and output.

In these cross sections hydrodynamic tubes of the total head [pressure] were established [erected] that are shifted by means of coordinates perpendicular to the long sides of the duct cross section. The determination of complete and static pressures took place by means of mercury-water manometers.

As a result of the flows in the MHD-generator ducts and the ducts of their models, optimum shape of the convergent channel [nozzle] and exit cone [diffusor] were found where the total coefficient of resistance is minimum. As an example, figure 12 shows the shapes and basic dimensions of such reducers. The length of the nozzle of the investigated ducts is recommended to be selected at (6-8) h, of the exit cone (15-20) h, where h is the height of the primatic section of the duct. Stabilization of flow in the prismatic section of the duct begins at a distance equal to (5-8) h from the input, the effect of the exit cone is propagated to (3-4) h upwards along the flow.

The graphs of the change in piezoelectric pressures (figure 13) make it possible to estimate the magnitude of the coefficient of friction λ applied to the calculation of resistance of the prismatic section of

the duct (λ = 0.012—0.015).

The equilibrium of hydraulic losses in the duct investigated (figure 12) is the following: the input reducer ~25%, the working sector ~25%, and the output reducer [adapter] ~50%.

From an examination of the characteristic dependences of $\eta = f(\mathrm{Re})$ (figure 14) it is evident that for similar flow circuits the region of hydraulic resistance, self-modeled according to the Reynolds number, is not attained. This is apparently explained by the characteristics of flow in the transition sectors and first [primarily] in the output (exit-cone) adapter.

According to the results of the flows, the conclusion is drawn of the necessity of preliminary experimental treatment of the flow circuit in the given range of operation according to the Reynolds numbers for the purpose of reducing the hydraulic losses and improving the flow structure in the duct.

References

1. Glukhikh, V.A. and Kirillov, I.R., *Magnetic Hydrodynamics*, 4, 107, 1966.

2. Cerini, D.J. and Elliott, D.G., Eigth Symposium of Engineering Aspects of Magnetohydrodynamics, Stanford, Mar 1967.

3. Vol'dek, A.I., NDVSh, *Electromechanics and Automation* (Elektromekhanika i avtomatika), 2, 120, 1959.

4. Sutton, G.W., Horowitz, H. Jr., Poritsky, H., Commun. and Electron., 58, 687, 1962.

Figures

1. Induction distribution of a magnetic field along the length of a single-wave MHD generator.

   1-noncompensating generator; 2,3-compensating short-circuited coil connected to a neutral phase; 4-compensating short-circuited coil and various capacitances and phases.

2. The efficiency of a single-wave MHD generator in the function of electric power output.

   1-a noncompensating generator; 2,3,4-generators with various compensation modes.

3. Operating characteristics of a helical MHD generator.

4. Experimental (1) and theoretical (2) power loss in liquid-metal for a helical MHD generator.

5. The dependence of β_1 on c_* and d_*.

6. The dependence of β_2 on c_* and d_*.

7. A no-load voltage DC generator.

8. Pressure operating in the duct of a DC generator.

9. Distribution of a field in a gap of a DC generator when $c_*=0$.

10. Distribution of a field in a gap of a DC generator when $c_*=0.8$.

11.* Distribution of a field in a gap of a DC generator when c_*=1.6.

12. The flow section of a model of the generator duct. 1-1, 2-2 are the cross-sections for measuring the velocity of the flow; 1-IV is the range of pressure samples; 1,2...8 are the sample pressure points.
    ' - position for the hydrodynamic tube .

13. Piezometric pressure curves.

14. Graph of the dependencies for $\zeta = \int(\mathrm{Re})$.

    Δ is the aerodynamic stand, $\cdot$ is the hydraulic stand.

* missing from the original preprint

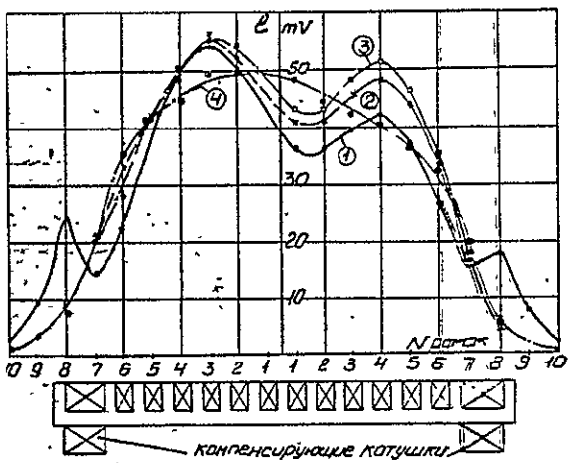

Рис. 1

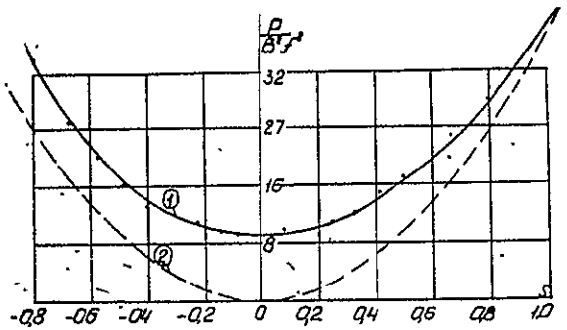

Рис. 4.

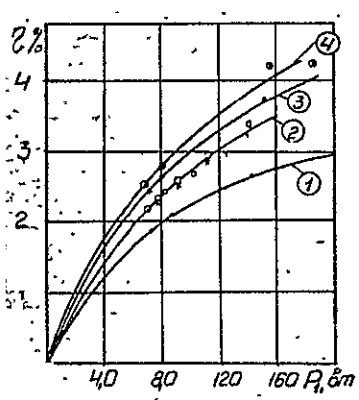

Рис. 2

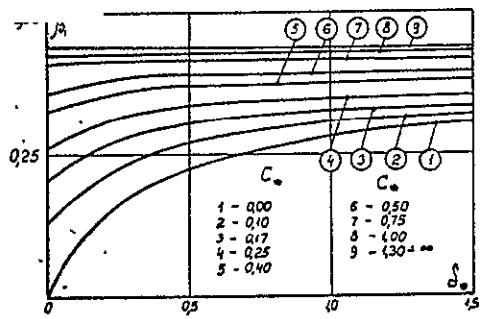

Рис. 5.

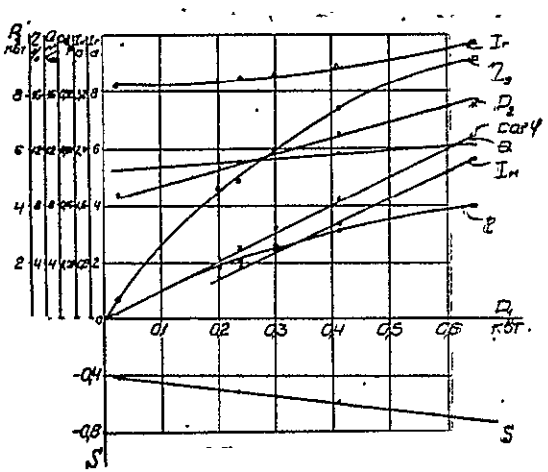

Рис. 3

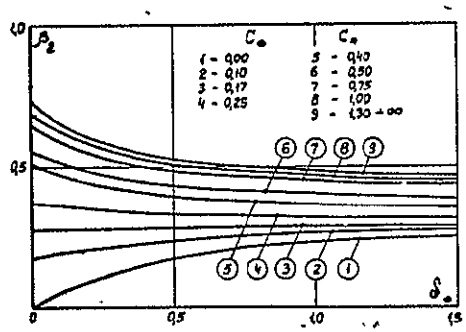

Рис. 6.
Зависимость β_2 от $C_к$ и $\delta_к$

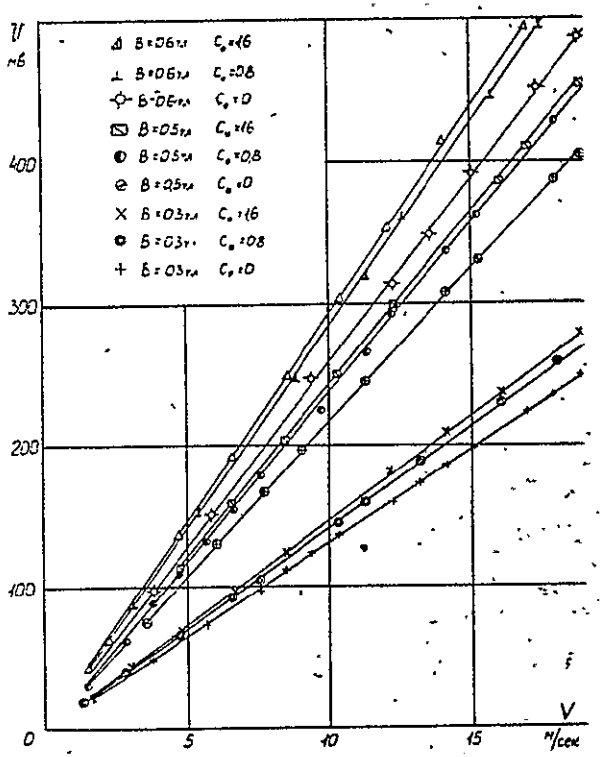

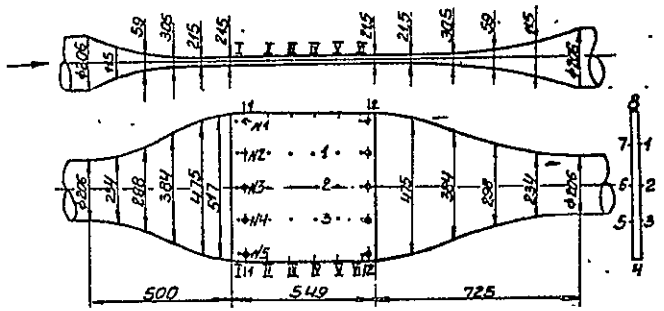

Рис.12.

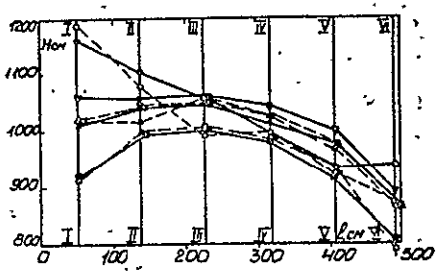

Рис.13.

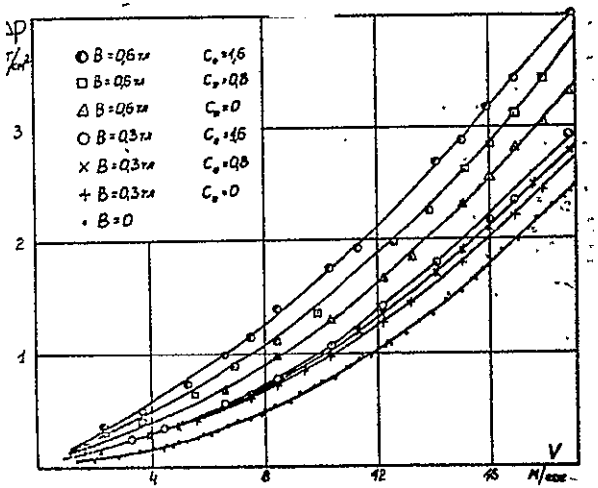

Рис.8

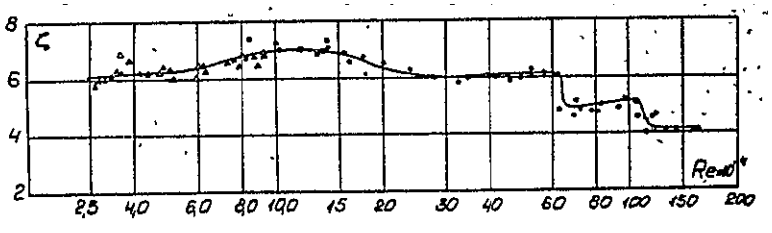

Рис.14.